Sustainable Nanocarbons via Biocatalysis of C-F Bond Cleavage by Electroactive Bacteria

Sarra Knani[1], Riad Ahmed Boughezal[1], Baptiste Cibron[1], Frédéric Barrière[1], Corinne Lagrost[1,2], Muriel Escadeillas[1], Ludivine Rault[2], Maida Costa de Oliveira[3], Paula E. Colavita[3] and James A. Behan[1].*

1 - Université de Rennes, CNRS, Institut des Sciences Chimiques de Rennes, UMR 6226, F-35000 Rennes, France.

2 - Université de Rennes, CNRS, ScanMAT, UAR 2025, F-35000 Rennes, France

3 - School of Chemistry, CRANN and AMBER Research Centres, Trinity College Dublin, College Green, Dublin 2, Ireland.

*email: james.behan@univ-rennes.fr

Abstract

Fluorographite is a promising starting material for the synthesis of graphene and graphene oxides via top-down exfoliation routes. C-F bonds in fluorographite can be chemically substituted to form graphene oxides with tuned surface chemistry. However, most defluorination routes reported proceed via fluorographene exfoliation from fluorographite followed by refluxing in organic solvents. Herein a one-pot, biogenic and aqueous route to graphene oxide nanomaterials directly from fluorographite with no pre-exfoliation step is demonstrated. Fluorographite incubation with the electroactive bacterial species *Geobacter sulfurreducens* yields water-dispersible graphene oxide quantum dots and partially-defluorinated graphene oxides as the main nanomaterial products in a single step. Biocatalysis at ambient temperature and pH proceeds through direct surface contact with bacteria through C-F bond

cleavage, with fluorographite serving as the sole electron acceptor for *exo*-electrogenic respiration. This bioexfoliation strategy presents a sustainable and green synthetic route to functionalised carbon nanomaterials with tuneable size and surface properties under ambient conditions.

Keywords: electroactive bacteria, biocatalysis, nanocarbons, bioexfoliation, fluorographene

1. Introduction

Fluorinated nanocarbons including fluorographenes have emerged as interesting materials for a variety of applications ranging from supercapacitors [1] and battery materials [2,3] to perovskite solar cells [4]. Historically the fluorination of graphite to form graphite fluoride ("fluorographite") produced excellent solid lubricant materials [5]. Nowadays fluorographite and its exfoliated derivatives are of great interest as composite materials in energy storage and conversion, catalysis and biosensing [6,7]. Though it was initially described as a 2-D analogue of polytetrafluoroethylene, it is now known that fluorographene is a reactive material suitable for the preparation of modified graphene materials [8–11]. This followed the first exfoliation of fluorographene from the bulk fluorographite in 2010 [12,13], along with its conversion to graphene under relatively mild conditions. The electrophilic carbons in fluorographene are susceptible to reductive defluorination and/or nucleophilic substitution [14], allowing for a remarkable variety of surface-modified or doped graphene materials to be prepared [6,10,15–17]. This top-down approach usually involves ultrasonication starting from graphite fluoride to yield the fluorographene, followed by reflux in organic solvents to eliminate fluorine and replace it with other moieties (**Figure 1 a**) [8–10,15,18–20]. Aqueous media routes to modified nanocarbons with fewer processing steps are therefore desirable, but are limited by the low water-solubility of the extremely hydrophobic fluorographite precursor.

Electroactive bacteria, *i.e.,* bacteria that can transfer electrons extracellularly, are capable of exchanging electrons with solid materials including electrodes and oxides of metals such as Fe(III) [21]. These redox processes are commonly anodic, i.e. involving the transfer of intracellular electrons derived from organic matter to an external electron acceptor, as found in iron-rich soils and the bioanodes of microbial fuel cell systems [22–25]. However it is also possible to develop cathodic systems, where

electrons are transferred from extracellular solids to the cell interior. Examples of this include Fe(II) oxidizing phototrophic bacteria, which can use Fe(II)-rich minerals as the electron source for anoxygenic photosynthesis [26,27]. When the capacity for extracellular electron transfer is applied to the synthesis of GO derivatives, the so-called 'bio-exfoliation' of GO usually involves the oxidation of dispersed graphite or graphene materials [28–30] where the starting material serves as the electron donor. For *Geobacter sulfurreducens* and related species electrons derived from the respiratory chain at the inner membrane are transferred to external solids via *c*-type cytochrome proteins which are localized at the outer membrane and secreted in the form of conductive protein nanowires which can carry electrons across long distances outside of the cell [22,31,32]. Another species of electroactive bacteria, *Shewanella oneidensis*, has been shown to reduce nanocarbons such as graphene oxide (GO) via its own extracellular respiratory machinery [33,34]. In both of these cases the extracellular solid serves as the terminal electron acceptor. Biological redox pathways may therefore serve as versatile routes to drive nanomaterial synthesis under mild conditions, including the synthesis of diverse nanocarbons with varied surface chemistry.

We hypothesized **(Figure 1 b**) that the relatively labile C-F bonds in graphitic fluorides could in principle serve as the electron acceptor for extracellular respiration by electroactive bacteria and hence potentially be cleaved via biocatalysis under mild, biocompatible conditions. Such a direct "bioexfoliation" route of bulk fluorographite to nanocarbons is unprecedented and would allow for the versatile surface chemistry of graphitic fluorides to be exploited to prepare GO and heteroatom-doped GO derivatives tailored to catalytic, imaging or biosensing applications under more sustainable conditions than those presently employed.

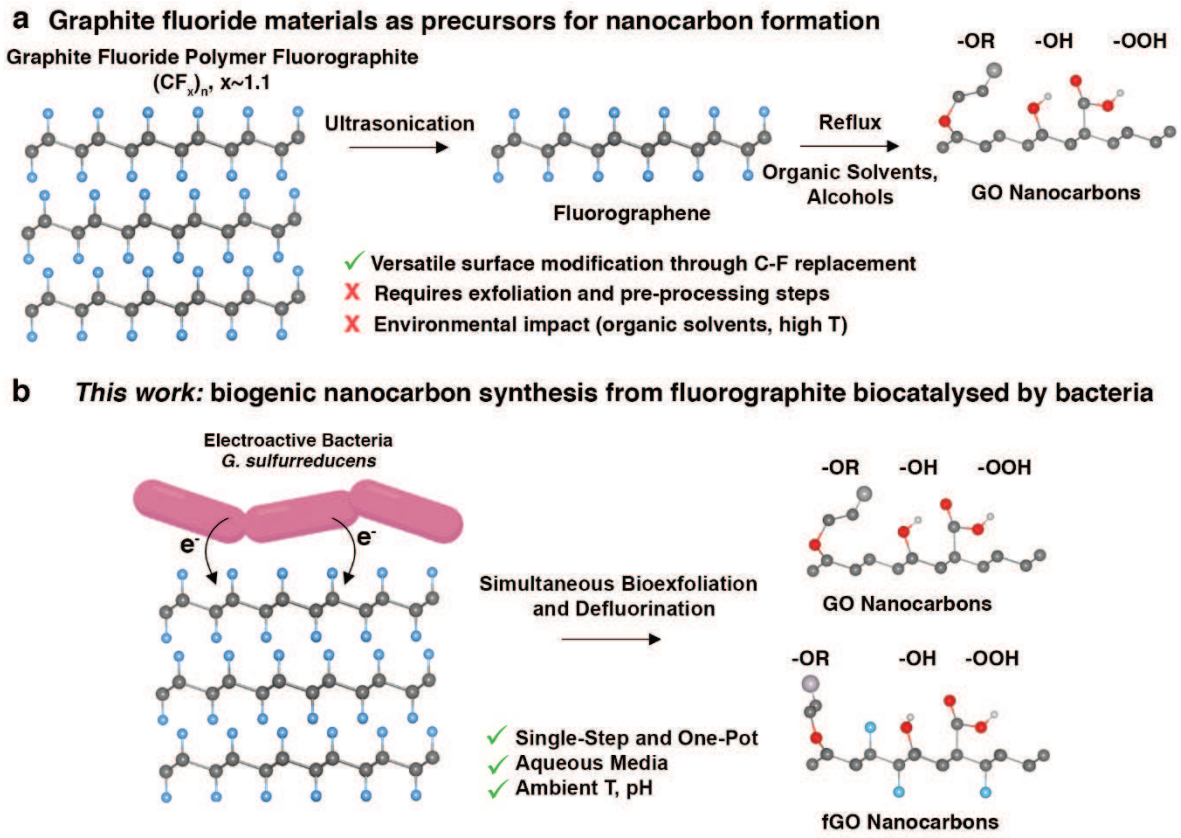

Figure 1. a) Illustrating a typical route to prepare GO nanocarbons from graphite fluoride precursors using ultrasonication to form fluorographene followed by organic solvent treatments to cleave C-F bonds. **b)** We present a one-pot biological route using the metabolic activity of electroactive bacteria to simultaneously bioexfoliate and cleave C-F bonds in fluorographite, forming a range of GO and fluorinated-GO nanocarbon products under ambient conditions in aqueous media.

In this work we present the simultaneous bioexfoliation and defluorination of bulk fluorographite to GO and partially-fluorinated GO (fGO) based nanocarbons biocatalysed by the electroactive bacterium *G. sulfurreducens*. The process operates at mild temperatures (35 °C) and at neutral pH, with no need for fluorographene exfoliation through ultrasonication methods. We find superior defluorination efficiencies with this biological method compared to previously reported abiotic routes applying physical exfoliation of fluorographite followed by high temperature reflux in organic solvents. A range of nanocarbons with tunable size, surface chemistry and fluorination degree are produced under aqueous conditions in a one pot incubation with only the bacteria, an organic electron donor, and the fluorographite as the presumed terminal electron acceptor for extracellular respiration. We show that the process is metabolically-driven, demonstrating a previously unknown capacity for these bacteria to biocatalytically cleave C-F. We propose a direct electron transfer mechanism from the bacteria to the fluorographite by outer-membrane cytochrome proteins at the bacteria surface. Reductive cleavage leads

to both defluorination and subsequent delamination of the graphitic starting material to produce valuable nanocarbon products, including ultrasmall graphene oxide quantum dots (GQDs), fGO nanoparticles and fluorographene sheets. Our results show how a biocatalytic approach can streamline the synthesis of nanomaterials with tailored physicochemical properties under ambient conditions.

2. Materials and Methods

2.1 Chemicals and Materials

Fluorographite (polymer, >61 wt. % F, Sigma Aldrich), sodium acetate (≥99%), riboflavin (Vitamin B2, ≥99%), sodium fumarate dibasic (≥99%), ammonium chloride (≥99.5%), potassium chloride (molecular biology grade (≥ 99.0%), NaH_2PO_4 (BioReagent, ≥98%), Na_2HPO_4 (ACS. ≥99.0%), Na_2SO_4 (≥ 99.0%), $MgCl_2 \cdot 6H_2O$ (BioReagent) and $CaCl_2 \cdot 2H_2O$ (BioXtra, ≥99.0%) and cytochrome *c* from equine heart were purchased from Sigma Aldrich. BBL™ Yeast extract was purchased from BD Biosciences. All chemicals were used as-received without further purification.

2.2. Culturing of *G. sulfurreducens* and Incubation with Fluorographite

G. sulfurreducens subsp. *sulfurreducens* strain PCA were anaerobically cultured in a modified acetate-fumarate media (the full media composition is given in **Supplementary Note 1** in the **Supplementary Information**) from cryostocks stored in 20% glycerol at –80 °C. Cultures were grown until the stationary phase, at which point the optical density at 600 nm (OD_{600}) was *ca.* 0.2 as measured using 1mL aliquots in quartz cuvettes via a dual-beam JASCO V-630 BIO spectrophotometer. The measured OD_{600} corresponds to a cell dry weight biomass of 0.66 g L^{-1} OD_{600}^{-1}, consistent with previous reports for *G. sulfurreducens* [35]. Cells were harvested by centrifugation at 5000×g for 10 minutes to pellet the bacteria followed by 3 washes with the desired incubation buffer. Minimal media contained only buffer (PBS or bicarbonate, pH 6.8-7) and 10 mM acetate and *G. sulfurreducens* at an OD_{600} of 0.4 in the presence of fluorographite (5-10 g/L). This media was also supplemented with 10 μM riboflavin as a redox shuttle in certain experiments as described in the main text. Biological replicates of the entire experiment were carried out three times starting from fresh cryostocks. All samples were incubated in darkness a thermostatic cabinet at 35 °C without agitation. Samples were regularly taken aseptically using an anoxic syringe to check the pH and optical density. Bacterial viability in the presence of flurographite was verified by adding 5 g/L of the powder to acetate-fumarate media, which did not affect

the apparent OD_{600} at *ca.* 0.2 after 3 days of growth. After the incubation the solution was centrifuged twice at 5000×g for 20 minutes to pellet bacteria and insoluble precipitated material, followed by treatment at 80 °C with 2% SDS and filter purification using 100 kDa MW cutoff Amicon® Ultra 15 mL filters to remove the incubation buffer and proteins. Experiments to demonstrate the presence of cytochrome proteins produced by the bacteria skipped the SDS treatment and removed the incubation buffer using 10 kDA MW cutoff Amicon® Ultra 15 mL filters while retaining the proteins and GQDs prior to characterization. The precipitates were washed 5 times with ultrapure water to remove incubation buffer and adherent biofilm prior to characterisation. Additional centrifugations at 20000×g for 3 cycles were applied to the colloids for size-selection of the resulting nanoparticles before TEM analysis. In all cases the final GQDs were concentrated to a volume of 5 mL in Millipore water using Amicon® filters and stored at room temperature prior to characterisation. The overall yield of bioexfoliated products, determined after oven-drying the products and unreacted starting material, was found to be 35 ± 5% based on 3 replicates after 9 days of incubation. This yield is comparable to previous works using ultrasonication, solvothermal intercalation [36] and ball-milling approaches [37] to prepare fluorographene.

2.3 Characterisation of fluorographite

UV-Visible spectroscopy characterisation

UV-Visible spectroscopy was carried out using a dual-beam JASCO V-630 BIO spectrophotometer using quartz cuvettes. Spectra were taken of purified GQDs in ultrapure water or directly in the growth media as described in the text. Pristine fluorographite was found to be nearly insoluble in water and was suspended in a 10% ethanol/water solution. All measurements are baseline-corrected using the dispersion medium as a blank.

Fluorescence spectroscopy characterisation

Fluorescence spectra were recorded on a Horiba Fluoromax® FM4 ET THERMO fluorimeter. GQDs were diluted in ultrapure water or anhydrous ethanol as described in the text. Emission spectra were recorded with an interval of 1 nm and a 5nm entrance/exit slit bandpass. Fluorescence intensities are presented after applying radiometric correction factors and normalised to the reference intensity to account for light source fluctuations.

X-ray Photoelectron spectroscopy characterisation

Samples for XPS analysis were prepared by depositing powder (0.05g) in the case of pristine fluorographite or precipitated material or by drop-casting purified GQD colloid solutions after dilution in anhydrous ethanol and drying in air. *p*-Doped Si wafers (1-5 Ω·cm resistivity, Siltronix) were used as substrates. XPS data were obtained using a NEXSA G2 (ThermoFisher Scientific) spectrometer using an Al Kα X-ray source working at 1486.6 eV with a spot size of 200 μm^2. Survey spectra (0–1000 eV) were acquired with an analyzer pass energy of 200 eV (1 eV/step, dwell time 10 ms); high-resolution spectra used a pass energy of 50 eV (0.1 eV/step, dwell time 50-300 ms). Charge compensation using a flood gun ($P = 4\times10^{-7}$ mbar) was applied to all powder preparations. The binding energies were corrected to the position of the C 1 s spectral component at 284.8 eV assigned to C-C and C-H species. Spectra were peak-fitted using commercial software (CasaXPS Version 2.3.25 PR1.0). Deconvolutions were performed using U 2 Tougaard background subtraction in all cases. Peak areas used in quantitative analysis were normalized by relative sensitivity factors provided by the manufacturer for atomic percentage determination (C 1 s = 1, O 1 s = 2.88, N 1s = 1.68, F 1s = 4.12).

Fourier transform infrared (FTIR) spectroscopy

FTIR measurements were performed using a JASCO FT/IR-4600 system. Dried power samples of flurographite and bioexfoliation products were pressed into KBr pellets and analysed versus a baseline of pure KBr. For all samples 35 scans were collected in the range of 4000 to 500 cm^{-1}.

Raman spectroscopy characterisation

Raman measurements were performed on drop-cast powders or GQD solutions dispersed in anhydrous ethanol on Si wafers and drying at room temperature. Measurements were carried out on a LabRAM HR Evolution from Horiba Scientific using a ×100 objective with a 523 nm laser with a 10s accumulation time at 1% laser intensity (0.15 mW power). The resulting spectra were deconvoluted using CasaXPS Version 2.3.25 PR1.0.

Transmission Electron Microscopy imaging

TEM images were acquired using a JEOL JEM 2100 HR transmission electron microscope equipped with a LaB_6 electron source with an acceleration voltage of 200 kV. A CCD Gatan Orius SC200D camera was used for conventional imaging while a CCD Gatan UltraScan 1000XP camera was used for

high-resolution images. Samples of purified GQDs were diluted in anhydrous ethanol and deposited by drop-casting on copper grids coated with carbon/formvar films followed by air drying.

Scanning Electron Microscopy imaging

SEM images were acquired using a JEOL JSM 7100 F electron microscope. Samples were prepared by drop-casting powders or colloid solution directly on *p*-doped Si wafers and rinsing 3 times with ultrapure water before drying in air followed by critical point drying and sputter-coating with gold prior to imaging.

Atomic Force Microscopy imaging

AFM was performed on drop-cast samples deposited on Si wafers. Measurements were carried out in semi-contact mode using an Ntegra NT-MDT AFM using NSG10 tips (NT-MDT) with a resonant frequency of 47 – 150 kHz and a force constant of 37.6 N/m. The resulting images were analysed using open-source software (Gwyddion® 2.65) using the following data processing operations: *level data by mean plane subtraction, shift mean value to zero* and *correct horizontal scars (strokes)*.

Fluoride Ion Detection

After incubation with electroactive bacteria the spent medium was crudely purified via centrifugation to remove large particles and bacterial cells prior to measurement with a F 800 fluoride ion sensitive electrode (ISE, supplied by WTW). The ISE was first calibrated with stock solutions of NaF with Total ionic strength adjustment buffer (TISAB II solution, Thermofisher®) from 10^{-5}-10^{-3} molar concentrations. (TISAB II, Thermofisher®) was added 1:1 to samples to allow comparability with standards.

3. Results and Discussion

To develop our method, we incubated fluorographite with a formula $(CF_x)_n$, x~1.1 (**Figure 2 a**) with *G. sulfurreducens* in a minimal medium consisting of a buffer (PBS or bicarbonate buffer, pH 7) supplemented with 10 mM acetate as the sole electron donor and fluorographite (5-10 mg/mL) as the sole electron acceptor. 10 µM riboflavin was added as a redox shuttle [38], though this was not found to be essential for bioexfoliation. **Figure 2 a)** shows the initial photograph directly after the reaction tubes were prepared. The white fluorographite powder is extremely hydrophobic and less dense than the liquid phase and floats at the liquid/gas interface. After 24h of incubation we identified regions of red

biofilm formation characteristic of *G. sulfurreducens* localised at the meniscus in contact with the fluorographite (**Figure 2 a**). A noticeable darkening of the white fluorographite at the interface is also evident along with a small amount of precipitation at the bottom of the tube. After 96 h of incubation the floating powder is noticeably grey in color, with a black layer of material forming at the surface of the liquid. No such changes were observed for the control tubes (**Figure 2 a** and **Figure S1**). The tubes were incubated for a further 6 d prior to the purification of the dispersion. At this point the solution had changed from the red color given by the *G. sulfurreducens* to a black-brown color consistent with colloidal nanocarbon dispersions.

3.1 Characterisation of biogenic GO derivatives produced from fluorographite

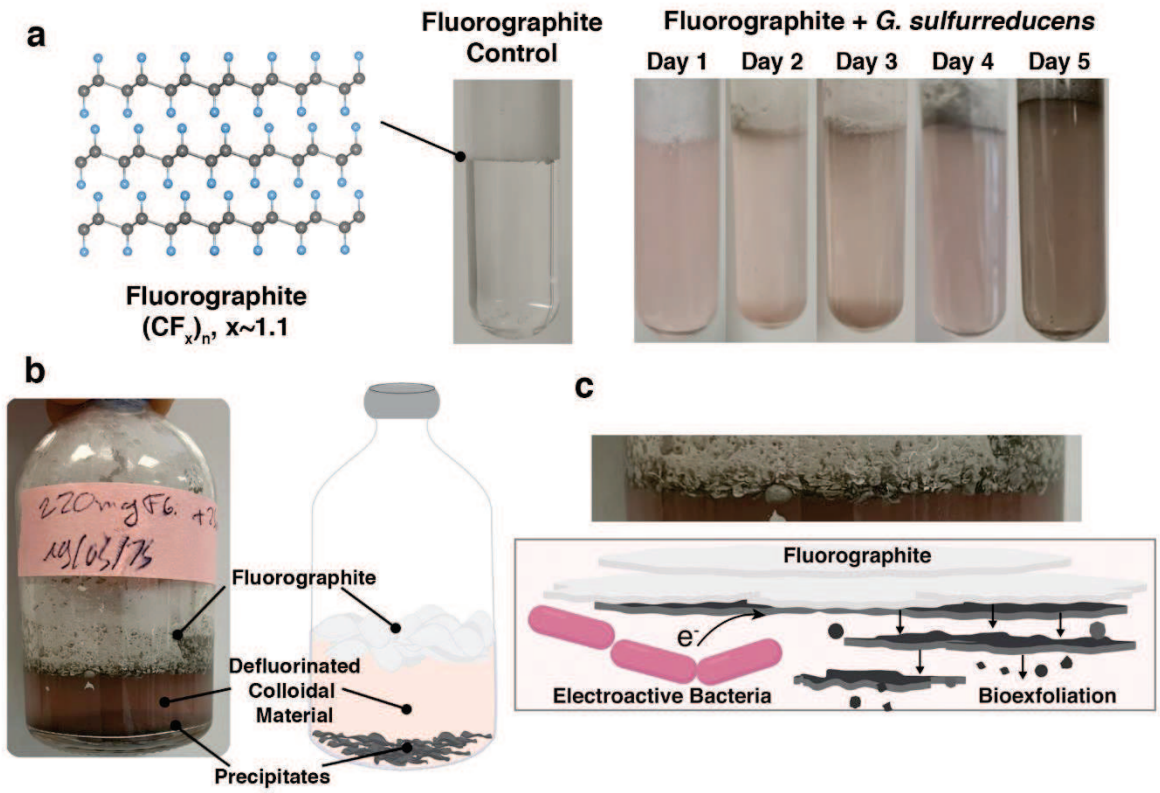

Figure 2 a) Representative photographs illustrating the evolution of fluorographite after incubation with *G. sulfurreducens* cultures over the course of 5 days. The control tube incubated in the same medium without bacteria is shown for reference and remained unchanged over the course of the experiment. **b)** Biological replicate of the experiment at a 25 mL scale. The fluorographite starting material, colloid and precipitate products are illustrated for clarity. **c)** Close up view of the fluorographite/media interface from **b).** A proposed mechanism the reduction and subsequent bioexfoliation of the fluorinated material through electron transfer from the electroactive bacteria at the interface is presented.

After incubation the reaction tubes contained a mix of colloidal dispersions of particles, precipitates at the bottom of the tubes and unreacted fluorographite (a representative example is shown in **Figure**

2 b) with our proposed bioexfoliation mechanism in **Figure 2 c**). The unreacted starting material was separated from the solution by pipetting and washed to remove salts and biomass prior to analysis. The morphology of fluorographite consists of heterogeneously distributed fragments ranging from hundreds of nm to microns in size based on SEM images (**Figure 3** a and **Figure S2 a).** Energy dispersive X-ray (EDS) mapping of the pristine material confirms the given C:F ratio of 1:1.1 (**Figure S3**). After removing the starting material, the colloid and precipitates were separated from one another by centrifugation and washing steps as described in the methods section. The total yield of bioexfoliated material was estimated at 35 ± 5% when harvested after 9 days of incubation. Henceforth we will focus on the characterisation of the dispersions, which contain exclusively defluorinated GQDs; the precipitates which are made up primarily of fGO materials with varied F content and morphology are characterized separately in **Supplementary Note 4**.

Drop-casting of the colloid taken directly from the reaction tubes of *G. sulfurreducens* treated samples onto silicon wafers after biomass removal reveals a mix of large aggregates and finer particles (tens of nm) as shown in **Figure 3 b-c** and **Figure S2 b-d**. EDS mapping of these smaller particles shows that they are composed of nearly equal atomic-% C and O with an apparent total absence of fluorine (**Figure S4** and **Table S4**). AFM measurements of the drop-casted particles yield step height estimates on the order of 3-4 nm (**Figure 3 d-e** with additional data presented in **Figure S5**). These results strongly suggest that incubating fluorographite with *G. sulfurreducens* results in both its defluorination and exfoliation to form carbon nanomaterials. To further confirm that defluorination occurred, we analysed the spent incubation medium after the bacterial treatment via fluoride-sensitive potentiometry (**Figure S6**). Results showed high mM concentrations of fluoride in bacteria-treated samples, with negligible concentrations measured for the pristine fluorographite.

3.2 Spectroscopic Characterisation of Biogenic Nanocarbons

The colloidal materials were further separated from larger particles by centrifugation at 20000×g and spin filtration using 10kDa MW filters as outlined in the methods. These GQDs were imaged by TEM (**Figure 3 f, h, i**), confirming the presence of nanoparticles < 10 nm in size. The histogram of particle sizes (**Figure 3 g**) gives an estimated average particle size of 3 ± 1 nm, similar to height profiles

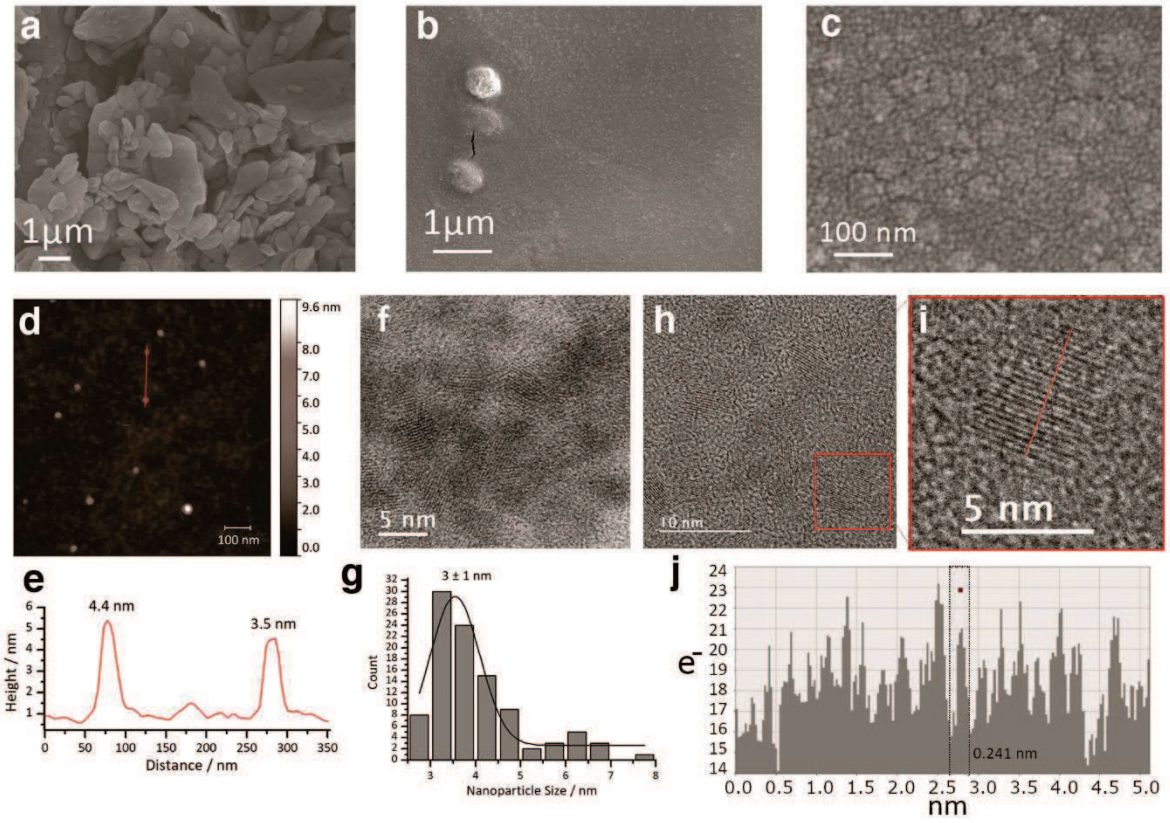

Figure 3. SEM images of **a)** fluorographite starting material **b)** – **c)** fluorographite after 7 days of incubation with *G. sulfurreducens*. **d)** AFM image of GQDs deposited on Si wafers. The height profile along with red line in d**)** is given in **e)**. **f)** HRTEM images of purified biogenic GQDs. **g)** histogram of GQD particle sizes estimated by measuring 100 GQDs across different areas of the TEM grid. **h)– i)** HRTEM images of GQDs. The inset in **i)** shows a HRTEM image of a single GQD showing its crystallinity and interplanar spacing of ~0.24 nm derived from the intensity profile **j)** taken along the white line in **i)**.

measured via AFM and consistent with GQDs. Fringes evident in high-resolution TEM (**Figure 3 h, i**) confirm the crystallinity of the particles; an interplanar spacing of ~0.24 nm is observed as shown in **Figure 3 j**, consistent with the expected value for the (1120) plane of graphite [39].

1

The colloidal dispersions after the removal of cells and spin filtration with 10 kDa MW cutoff filters retained the distinct pale red color characteristic of *G. sulfurreducens* cultures (**Figure S7 a)**, which suggests the presence of cytochrome proteins. BCA assays confirmed *ca.* 50 µg/mL protein remaining in GQD solutions after the removal of cells and biomass by centrifugation. UV-Visible spectroscopy on these crude products (**Figure S7 b**) showed features characteristic of *c*-type cytochromes. These proteins remained even using 100 kDa MW cutoff filters, consistent with outer membrane cytochromes produced by *G. sulfurreducens* which are known to self-assemble into larger structures such as protein nanowires [31,40]. We removed all proteins from these dispersions by a denaturing treatment in 2% SDS at 80 °C followed by centrifugal filtration with 100 kDa MW filters. The purified GQD dispersions were

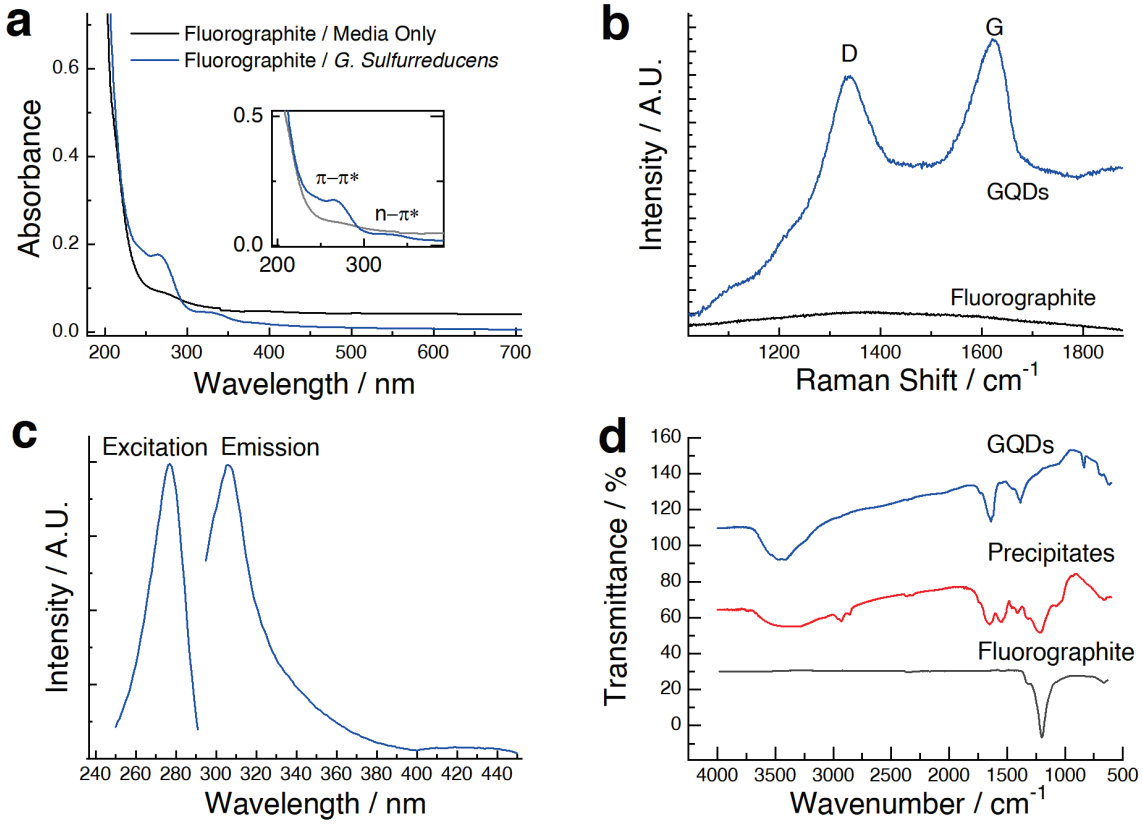

Figure 4 a) UV-Visible spectra of a GQD solution prepared from treatment of fluorographite with *G. sulfurreducens* in PBS/Acetate media. Spectra of fluorographite incubated under identical conditions in media only are presented as a control. The inset highlights the region between 200-500 nm where distinct π→π* and n→π* transitions are evident in the bacteria-treated sample only. **b)** Raman spectrum (532 nm laser excitation) of the GQDs presented in **a)** and pristine fluorographite. **c)** Fluorescence excitation and emission spectra of the GQDs dispersed in ultrapure water recorded using an excitation wavelength of 250 nm. **d)** FTIR spectra of pristine fluorographite, precipitates after incubation with *G. sulfurreducens* and purified GQDs.

then characterized by a combination of UV-Visible, FTIR, Raman and fluorescence spectroscopy. The UV-Visible absorbance spectrum of purified GQDs shown in

Figure 4 a) shows the appearance of distinct peaks at ~260 nm and ~330 nm, assigned to $\pi \rightarrow \pi^*$ and $n \rightarrow \pi^*$ transitions respectively [41,42]. The $\pi \rightarrow \pi^*$ transitions are typically assigned to aromatic sp^2 domains while $n \rightarrow \pi^*$ transitions are normally assigned to surface states which arise at edges functionalised with oxygen groups[43]. Abiotic controls of fluorographite incubated in the minimal media yielded only a broad absorbance close to 200 nm, similar to dispersions of the untreated starting material (**Figure S8**). This suggests that the fluorinated starting material remains stable in the absence of *G. sulfurreducens*.

Raman spectroscopy of the GQDs in

Figure 4 b) shows typical D and G peak features of disordered carbon nanomaterials, while very weak signals were obtained for fluorographite, as expected for highly fluorinated carbons [12,44]. The D peak – associated to disordered features in the carbon scaffold such as defects, edges and impurities – appears at a typical value of ~1335 cm^{-1} while the G peak is blue-shifted from its typical region of ~1580 cm^{-1} to ~1620 cm^{-1}. This shift is typical of graphene oxides with a high degree of sp^3 carbons[45] and suggests that the GQDs are highly defective and/or oxidized[46]. This result is consistent with the D to G peak intensity ratio, I_D/I_G estimated through the deconvolution of the Raman spectra of GQDs presented in **Figure S9** and **Table S5**. The I_D/I_G is indicative of the degree of disorder in the carbon scaffold in carbon materials. The estimated ratio of 1.7 for our GQDs is typical of GO (see **Table S6** and References [47,48]).

It is well-known that GQDs possess fluorescent properties depending on variables such as particle size, sp^2 cluster size and defect states or surface traps[43,49,50]. The fluorescent properties of the GQDs dispersed in water are summarised in **Figure 4 c**. The purified GQDs were found to be UV-fluorescent with an emission maximum observed at 306 nm (~4.06 eV) and excitation maximum at 280 nm (4.4 eV). No significant fluorescence was observed for control samples of fluorographite incubated in acetate medium only (**Figure S10**). This deep-UV emission maximum is among the shortest emission

wavelengths ever reported for GQDs, with only the microwave-assisted GQDs prepared by Tang et al. having a higher emission energy at 4.1 eV [49].

We also found that the fluorescence emission maximum of the GQDs shifted significantly from 333 nm to 306 nm with little change in the fluorescence intensity after the removal of cytochrome proteins by SDS treatment (**Figure S10).** An almost identical shift was found when crude GQDs were transferred into ethanol without removing the proteins (**Figure S11**), suggesting that the fluorescence is linked to surface states and/or solvent interactions rather than any direct contribution from the proteins themselves.

FTIR studies were carried out on the starting fluorographite material as well as on both the precipitates and the purified colloidal phase after biomass removal (**Figure 4 d**). The FTIR spectrum of the GQDs is consistent with previous reports on GO materials[51], showing peaks attributed to O-H (~3700 – 3000 cm^{-1}), C=O (~1700 cm^{-1}) and C=C (~1600 cm^{-1}). Importantly, the sharp peak attributed to C-F species at around 1200 cm^{-1} [52] is prominent in the starting material, diminished in the precipitates and entirely absent in GQDs, suggesting fluorine elimination in the biogenic nanomaterials and the formation of new nanocarbon materials terminated with oxygen moieties[52,53].

X-ray Photoelectron Spectroscopy measurements were used to quantitatively follow the defluorination of the starting material and to characterise the surface chemistry of the resulting GQDs. Survey spectra of *G. sulfurreducens* treated fluorographite compared to abiotic controls and the fluorographite starting material are given in **Figure 5 a)**. Aside from peaks associated to the Si substrate[54], the major elements present for the pristine material and abiotic control are C, F and O. Area ratios taken from high-resolution scans (**Figure 5 b, d-e** and **Figures S12** and **S13**) were used to calculate the O/C, N/C and F/C ratios summarised in **Table 1**. For both pristine fluorographite and abiotic controls a single intense F 1s peak is observed around 688 eV (**Figure 5 b**). The F/C is 1.1 for the starting material, in agreement with the SEM-EDX analysis reported in **Figure S4**). Incubating the fluorographite in 10 mM acetate medium only slightly reduces the F/C ratio to 1.0, which is more likely attributed to adventitious carbon contamination than to a loss of F, since the O/C ratio of the control remains unchanged from the value of the as-received powder of ~0.1. By contrast, high-resolution scans of the F 1s region (**Figure 5 b**) for the *G. sulfurreducens* treated sample shows a total absence of F in the survey spectrum. This result was

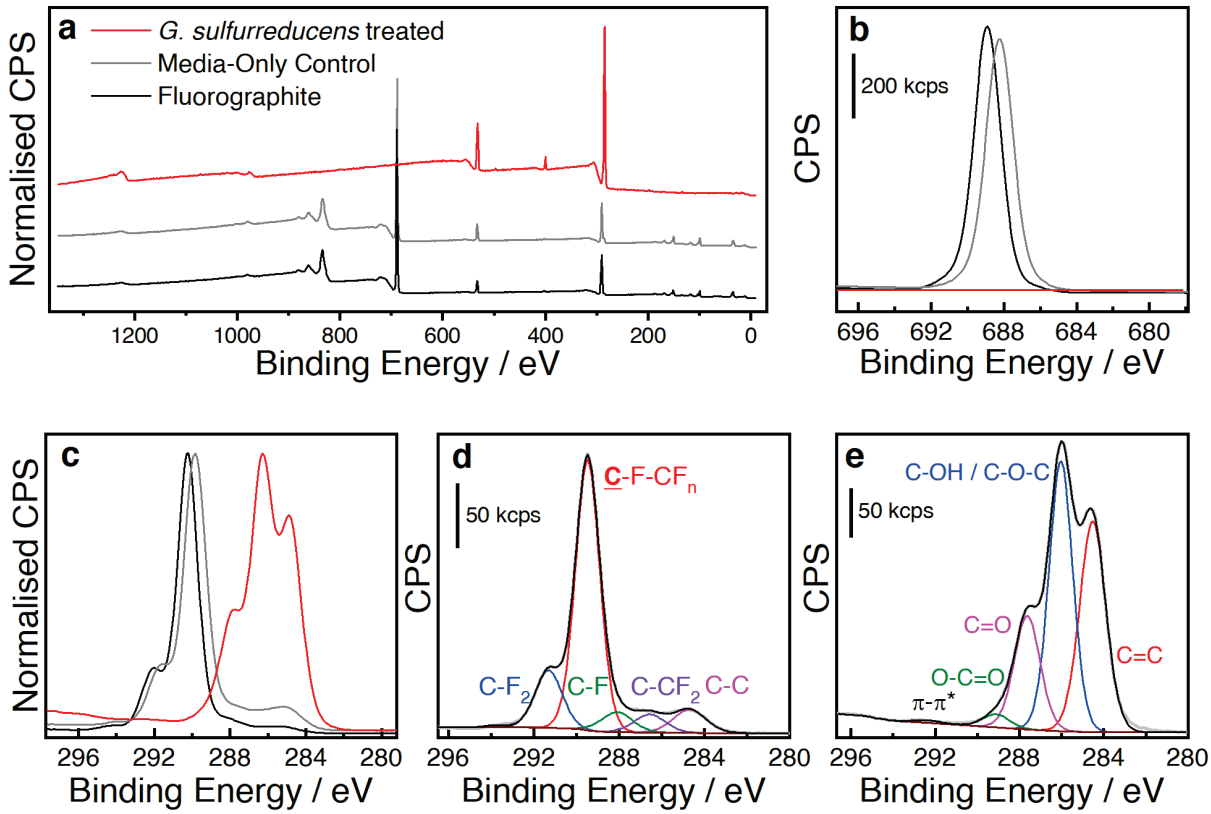

Figure 5 a) Survey spectra of GQDs prepared by incubation of fluorographite with *G. sulfurreducens*, fluorographite incubated in media only and pristine fluorographite. Spectra are normalised by the maximum counts per second (CPS) and presented offset from one another for clarity. **b)** High-resolution core level spectra in the F 1s region for *G. sulfurreducens* treated fluorographite compared to control and pristine samples, showing total defluorination of the samples occurs only when co-incubated with the electroactive bacteria. **c)** High-resolution core-level spectra in the C 1s region of *G. sulfurreducens* treated fluorographite, compared to the media-only control and pristine sample. Peak-fitted spectra of **d)** pristine fluorographite and **e)** *G. sulfurreducens* treated fluorographite.

reproduced across numerous batches (**Figure S15**) and confirms that the biogenic GQDs are fluorine-free. Further evidence for defluorination is found in high-resolution core-level spectra in the C 1s region (**Figure 5 c**). For both untreated and abiotic control samples, the main C 1s peak is centered around 291 eV consistent with fluorinated carbons [55], while that of *G. sulfurreducens* treated fluorographite is shifted closer to 286 eV as expected for GO[56]. Peak-fitted spectra are presented in **Figure 5 d-e** and **Figure S12**. For control and pristine samples, the predominant contributions are C-F-CF_n, C-F_2 and C-F species [57] with a lower binding energy contribution most likely due to adventitious carbon contamination. The C 1s region measured for GQDs produced by *G. sulfurreducens* treatment shows

peaks centered at 284.5 eV, 286.2 eV and 287.8 eV consistent with graphitic C=C, C-O and C=O contributions respectively [56].

Sample	C at. %	O at. %	N at. %	F at. %	O/C	N/C	F/C
Fluorographite	43.9	5.0	0.4	50.7	0.11	0.009	1.1
Abiotic Control	44.9	6.1	0.7	48.3	0.13	0.014	1.0
G. sulfurreducens treated	61.9	30.9	7.2	0	0.49	0.1	0

Table 1. Elemental composition ratio of fluorographite and GQD samples derived from XPS analysis.

This result combined with the dramatic increase in the O/C from ~0.1 to ~0.5 points to a replacement of C-F surface groups primarily by oxygen moieties. Finally, the increase of the N/C from ~0.01 to 0.1 may be due to residual proteins or organic matter arising from bacteria which remain detectable by XPS even after purification.

3.3 The role of riboflavin as a redox shuttle

It is well-known that C-F linkages in exfoliated fluorographene can be replaced with other moieties under relatively mild conditions [14]. In particular, the reaction of C-F with amines has been suggested as a route towards nitrogenated carbons [8,58]. Recently Siedle *et al.* proposed a redox mechanism for this process whereby fluorinated carbon serves as an electron acceptor and defluorination produces radical intermediates which then react with amines or other co-reactants to produce the modified carbon surface [18].

In the case of *G. sulfurreducens,* the *exo*-electrogenic redox behaviour involves membrane cytochrome proteins and external conductive protein nanowires which allow for electrons derived from intracellular respiratory processes to be transferred to external, solid electron acceptors [22,31]. It is already certain that our incubation conditions encourage the production of abundant *c*-type cytochromes based on UV-Visible spectra of crude colloidal products presented in **Figure S7**. Considering that the media used for fluorographite incubation contains acetate as an electron donor and fluorographite as an acceptor, we hypothesise that defluorination occurs through direct electron transfer of bacteria attached at the fluorographite surface (**Figure 2 c**) using these secreted cytochromes. This would explain the

visible changes in appearance of the fluorographite localised at the interface between the starting material and the *G. sulfurreducens* in solution in **Figure 2 a)** and **b)**.

However, soluble redox shuttles such as flavins can also facilitate indirect electron transfer between surface cytochromes and electron acceptors [38], without the need for bacterial adhesion. We ruled out direct fluorographite modification by riboflavin in the absence of bacteria using media-only controls which used 10 μM riboflavin as a redox shuttle without adding *G. sulfurreducens* (see **Figure 4a**, **Figure 5**, and **Figures S1** and **S10** in the Supporting Information). Hence, while amines can directly replace C-F in fluorinated graphenes using more aggressive treatments [8], this does not appear to occur under the mild and biocompatible conditions employed here. To investigate the contribution of riboflavin to the observed bioexfoliation, we carried out experiments using media containing only 10 mM acetate and PBS as a buffer. TEM imaging and spectroscopic analysis of riboflavin-free GQDs is reported in **Figure Figure 6**, with additional characterization reported in **Supplementary Note 3**. As **Figure 6 a-d** shows, we found comparable particle sizes and almost identical spectroscopic responses for GQDs prepared in media supplemented with and without the mediator. XPS analysis reported in **Figure S15** and **Table S7** show comparable surface chemical composition of riboflavin-free GQDs. Hence riboflavin addition is not essential for bio-exfoliation by *G. sulfurreducens*. We observed a more rapid onset of apparent bioexfoliation when 10 μM riboflavin was present (compare the visual appearance of riboflavin-free samples in **Figure S14** with those incubated with riboflavin addition shown in **Figure 2 a**, both after 3 days of incubation with *G. sulfurreducens*) which indicates a likely role in increasing the efficiency of electron transfer by redox shuttling, as has been observed for Fe(III) bioreduction by electroactive bacteria [38].

In addition to the colloidal dispersions discussed above, incubation of fluorographite with *G. sulfurreducens* also produced black precipitates at the bottom of the reaction tubes. These are characterised in **Supplementary Note 4.** SEM-EDX analysis of the precipitates presented in **Figure S16** shows particles ranging from tens of nm to multiple microns in size with a wide range of F/C values between 0.2-0.6, consistent with fGO. Structures resembling graphene nanoplatelets and other layered structures were identified in TEM images (**Figure S17**), suggesting that the biogenic protocol can

produce a variety of carbon nanostructures with differing surface termination and morphology without the need for ultrasonication or agitation. The presence of residual fluorine in these bioexfoliated

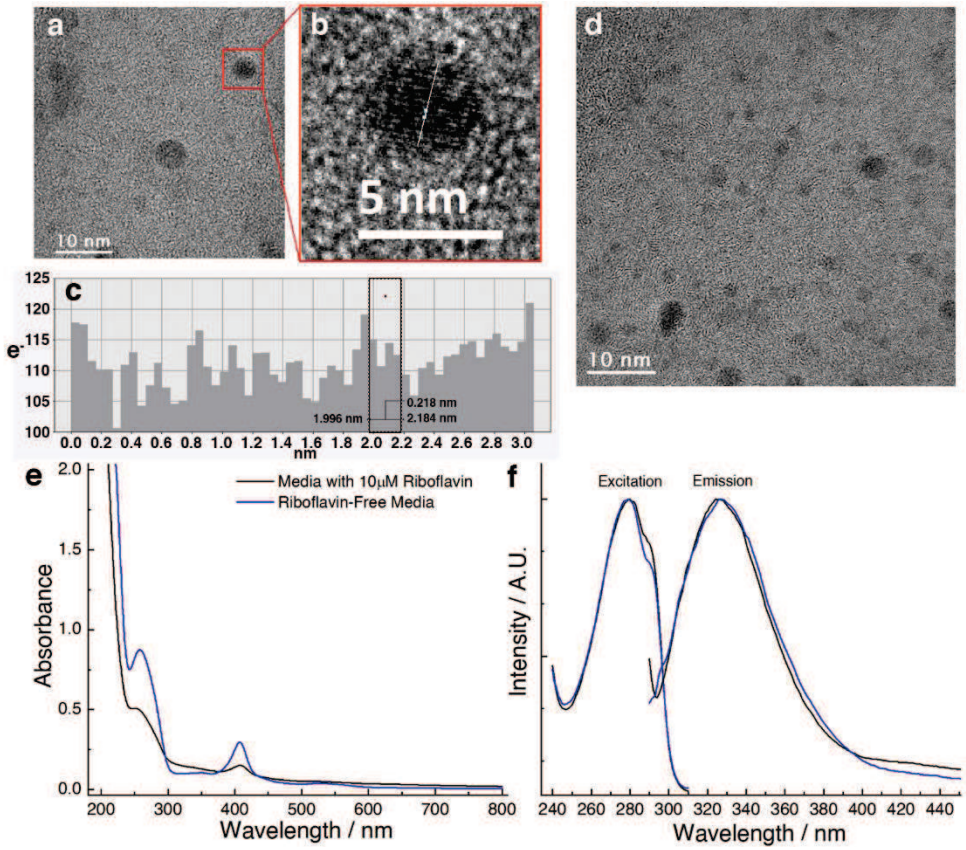

materials ranging

Figure 6 a) TEM images of GQDs prepared from fluorographite in acetate media without riboflavin addition. **b)** HRTEM image of a single GQD taken from the bounded region shown in red in **a)**. **c)** intensity profile taken along the white line in **b)** from which an interplanar spacing of *ca.* 0.22 nm was found. **d)** shows additional TEM images from the same batch of riboflavin-free GQDs. **e)** UV-Visible and **f)** fluorescence spectra of GQDs produced from *G. sulfurreducens* treatment of fluorographite with and without the addition of 10 μM riboflavin to the growth media. Spectra were obstained on crude GQD products without the removal of cytochrome proteins. The sample containing 10 μM riboflavin is a biological replicate of the experiments reported in Figures 2-5.

from 10-25 atomic % is of broad interest for the synthesis of heteroatom-modified nanocarbons, as these C-F groups can be potentially substituted with C-O, C-N or C-S linkages[8–11,18].

Top-down methods for the production of GO derivatives from graphite almost universally require harsh physical and chemical treatments such as ultrasonication to exfoliate graphene layers, followed by oxidative or thermal treatments to modify the carbon surface or to produce smaller graphitic entities including GQDs. Fluorinated graphites offer an alternative route to versatile surface modifications by cleaving C-F, but synthetic routes to GO or GQDs reported so far require exfoliation to fluorographene in organic solvents such as DMF, acetonitrile and ethanol, followed by reflux or prolonged acid/base

treatments [8–10,59,60]. This is because fluorographite itself remains stable indefinitely [18], a fact affirmed in our control studies, where it retains essentially all of its F content under abiotic conditions regardless of the media composition. To explain the rapid degradation of fluorographite in the presence of *G. sulfurreducens,* we propose a single-step redox mechanism catalysed by the electroactive bacteria which simultaneously defluorinates fluorographite while producing both GQDs and partially-defluorinated GO materials. This mechanism, illustrated schematically in **Figure 2 c)**, involves no liquid phase exfoliation methods such as ultrasonication to delaminate fluorographene. Defluorination is instead initiated by electron transfer to the fluorographite [14,18,61]. Previous evidence of direct reductive C-F removal was shown only at high temperatures from 95 – 200 °C with as much as 3% fluorine remaining in the products [18], while another aqueous method reported for C-F bond cleavage of fluorographite used radical chemistry to both defluorinated the material and produce a range of nanomaterials including nanoplatelets similar to those characterized in this work [62].

The total defluorination of fluorographite we observe at ambient temperatures suggests that the reduction is efficiently catalysed at the bacteria-fluorographite interface. This suggests a previously-unknown biocatalytic role for the outer membrane proteins of *G. sulfurreducens* in C-F cleavage. Further work is necessary to elucidate the specific roles of proteins such as outer membrane cytochromes which are likely involved in relaying electrons from the bacteria to the fluorographite.

Assuming fluorographite degradation proceeds through *exo*-electrogenic respiration by bacteria in direct surface contact, the redox potential of fluorographite must be sufficiently high in order to accept electrons from membrane cytochromes, for which the formal potential $E^{0'}$ has been estimated at *ca.* -200 mV [22]. There are varying reports of the redox potential for fluorographite; Yaokawa *et al.* found that electrochemical defluorination of $CF_{1.1}$ in fluoride-ion batteries can occur at -0.14 V vs SHE [63] while Siedle *et al.* report the reduction of defective fluorographite by decamethylosmocene at potentials as high as +0.64 V vs SHE [18]. It is already known from studies with polarised electrodes that *G. sulfurreducens* can develop rich biofilms at potentials as low as -0.15 V vs SHE [64,65]. Hence it is plausible that fluorographite serves as the terminal electron acceptor for electrons ultimately derived from acetate through metabolism by *G. sulfurreducens*. This mechanism also explains the presence of

partially defluorinated GO materials found in the precipitates. Reductive defluorination by the bacteria produces partially-fluorinated fGO particles which are soluble enough to precipitate and subsequently undergo further reductive cutting and defluorination by the bacteria to produce smaller nanostructures. In the limit this results in ultrasmall fluorine-free GQDs.

4. Conclusions

We have presented a sustainable, biogenic route to GO from fluorographite which involves the apparent biocatalysis of C-F cleavage at low temperature and neutral pH. Direct contact between electroactive bacteria and fluorographite is required for this bioexfoliation, suggesting a catalytic role for specific outer membrane proteins in defluorination which has never previously been observed. This route eliminates the need for organic solvents and for ultrasonication, as bioexfoliation proceeds directly from the graphitic starting material in aqueous media. We anticipate that this protocol will provide new, green routes to nanocarbons with size and surface chemistry tailored to particular applications in sensing, optics and electrocatalysis.

CRediT authorship contribution statement

Declaration of competing interest

The authors declare that they have no known competing financial interests or personal relationships that could have appeared to influence the work reported in this paper.

Acknowledgements

This work was partially supported by the “PHC ULYSSES” program (project number: 48456XA), funded by the French Ministry for Europe and Foreign Affairs and Taighde Eireann – Research Ireland. This project has received financial support from the CNRS through the MITI interdisciplinary programs. This work was funded by the French National Research Agency (ANR-25-CE50-4529-01 HYBNA). The Raman, TEM and XPS measurements have been performed on the SIR, THEMIS and ASPHERYX platforms at UR, respectively. L. Joanny is acknowledged for SEM images performed at

the CMEBA platform (ScanMAT, UAR 2025 Université de Rennes-CNRS). The authors thank C. Poriel and C. Quinton for providing access to spectroscopy instruments.

TOC Figure:

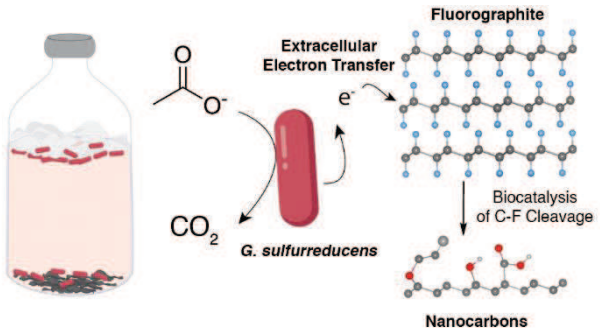

References

[1] H. An, Y. Li, P. Long, Y. Gao, C. Qin, C. Cao, Y. Feng, W. Feng, Hydrothermal preparation of fluorinated graphene hydrogel for high-performance supercapacitors, Journal of Power Sources 312 (2016) 146–155. https://doi.org/10.1016/j.jpowsour.2016.02.057.

[2] D. Damien, P.M. Sudeep, T.N. Narayanan, M.R. Anantharaman, P.M. Ajayan, M.M. Shaijumon, Fluorinated graphene based electrodes for high performance primary lithium batteries, RSC Adv. 3 (2013) 25702–25706. https://doi.org/10.1039/C3RA45377D.

[3] R. Yaokawa, K. Mukai, T. Nonaka, S. Kosaka, N. Ogihara, Redox Reaction Mechanism of Graphite Fluoride (CF)n in Fluoride-Ion Batteries, Chem. Mater. 35 (2023) 10584–10593. https://doi.org/10.1021/acs.chemmater.3c02217.

[4] C. Hanmandlu, M. Sahoo, C.-C. Liu, H.-A. Chen, C.-W. Pao, Y.-C. Chang, C.-W. Chu, C.-S. Lai, Few-layer fluorine-functionalized graphene hole-selective contacts for efficient inverted perovskite solar cells, Chemical Engineering Journal 430 (2022) 132831. https://doi.org/10.1016/j.cej.2021.132831.

[5] R.L. Fusaro, H.E. Sliney, Graphite Fluoride (CFx)n—A New Solid Lubricant, A S L E Transactions 13 (1970) 56–65. https://doi.org/10.1080/05698197008972282.

[6] R.A. Borse, M.B. Kale, S.H. Sonawane, Y. Wang, Fluorographene and Its Composites: Fundamentals, Electrophysical Properties, DFT Studies, and Advanced Applications, Advanced Functional Materials 32 (2022) 2202570. https://doi.org/10.1002/adfm.202202570.

[7] X. Chen, K. Fan, Y. Liu, Y. Li, X. Liu, W. Feng, X. Wang, Recent Advances in Fluorinated Graphene from Synthesis to Applications: Critical Review on Functional Chemistry and Structure Engineering, Advanced Materials 34 (2022) 2101665. https://doi.org/10.1002/adma.202101665.

[8] D. Zaoralová, V. Hrubý, V. Šedajová, R. Mach, V. Kupka, J. Ugolotti, A. Bakandritsos, M. Medved', M. Otyepka, Tunable Synthesis of Nitrogen Doped Graphene from Fluorographene under Mild Conditions, ACS Sustainable Chem. Eng. 8 (2020) 4764–4772. https://doi.org/10.1021/acssuschemeng.9b07161.

[9] R.A. Borse, M.B. Kale, S.H. Sonawane, Y. Wang, Fluorographene and Its Composites: Fundamentals, Electrophysical Properties, DFT Studies, and Advanced Applications, Advanced Functional Materials 32 (2022) 2202570. https://doi.org/10.1002/adfm.202202570.

[10] M. Dubecký, E. Otyepková, P. Lazar, F. Karlický, M. Petr, K. Čépe, P. Banáš, R. Zbořil, M. Otyepka, Reactivity of Fluorographene: A Facile Way toward Graphene Derivatives, J. Phys. Chem. Lett. 6 (2015) 1430–1434. https://doi.org/10.1021/acs.jpclett.5b00565.

[11] D.D. Chronopoulos, A. Bakandritsos, M. Pykal, R. Zbořil, M. Otyepka, Chemistry, properties, and applications of fluorographene, Applied Materials Today 9 (2017) 60–70. https://doi.org/10.1016/j.apmt.2017.05.004.
[12] R.R. Nair, W. Ren, R. Jalil, I. Riaz, V.G. Kravets, L. Britnell, P. Blake, F. Schedin, A.S. Mayorov, S. Yuan, M.I. Katsnelson, H.-M. Cheng, W. Strupinski, L.G. Bulusheva, A.V. Okotrub, I.V. Grigorieva, A.N. Grigorenko, K.S. Novoselov, A.K. Geim, Fluorographene: A Two-Dimensional Counterpart of Teflon, Small 6 (2010) 2877–2884. https://doi.org/10.1002/smll.201001555.
[13] R. Zbořil, F. Karlický, A.B. Bourlinos, T.A. Steriotis, A.K. Stubos, V. Georgakilas, K. Šafářová, D. Jančík, C. Trapalis, M. Otyepka, Graphene fluoride: a stable stoichiometric graphene derivative and its chemical conversion to graphene, Small 6 (2010) 2885–2891. https://doi.org/10.1002/smll.201001401.
[14] K.E.Jr. Whitener, R. Stine, J.T. Robinson, P.E. Sheehan, Graphene as Electrophile: Reactions of Graphene Fluoride, J. Phys. Chem. C 119 (2015) 10507–10512. https://doi.org/10.1021/acs.jpcc.5b02730.
[15] J. Sturala, J. Luxa, M. Pumera, Z. Sofer, Chemistry of Graphene Derivatives: Synthesis, Applications, and Perspectives, Chemistry – A European Journal 24 (2018) 5992–6006. https://doi.org/10.1002/chem.201704192.
[16] V. Hrubý, D. Zaoralová, M. Medveď, A. Bakandritsos, R. Zbořil, M. Otyepka, Emerging graphene derivatives as active 2D coordination platforms for single-atom catalysts, Nanoscale 14 (2022) 13490–13499. https://doi.org/10.1039/D2NR03453K.
[17] W. Feng, P. Long, Y. Feng, Y. Li, Two-Dimensional Fluorinated Graphene: Synthesis, Structures, Properties and Applications, Advanced Science 3 (2016) 1500413. https://doi.org/10.1002/advs.201500413.
[18] A.R. Siedle, Y. Losovyj, J.A. Karty, D. Chen, K. Chatterjee, V. Carta, B.D. Stein, U. Werner-Zwanziger, C–F Bond Activation in the Solid State: Functionalization of Carbon through Reactions of Graphite Fluoride with Amines, J. Phys. Chem. C 125 (2021) 10326–10333. https://doi.org/10.1021/acs.jpcc.1c00734.
[19] X. Ye, L. Ma, Z. Yang, J. Wang, H. Wang, S. Yang, Covalent Functionalization of Fluorinated Graphene and Subsequent Application as Water-based Lubricant Additive, ACS Appl Mater Interfaces 8 (2016) 7483–7488. https://doi.org/10.1021/acsami.5b10579.
[20] L. Yang, Y. Li, L. Wang, Y. Pei, Z. Wang, Y. Zhang, H. Lin, X. Li, Exfoliated Fluorographene Quantum Dots as Outstanding Passivants for Improved Flexible Perovskite Solar Cells, ACS Appl. Mater. Interfaces 12 (2020) 22992–23001. https://doi.org/10.1021/acsami.0c04975.
[21] T. Philippon, F.-Z. Ait-Itto, A. Monfort, F. Barrière, J.A. Behan, Fe(III) oxide microparticles modulate extracellular electron transfer in anodic biofilms dominated by bacteria of the Pelobacter genus, Bioelectrochemistry 151 (2023) 108394. https://doi.org/10.1016/j.bioelechem.2023.108394.
[22] T. Ueki, Cytochromes in Extracellular Electron Transfer in Geobacter, Appl Environ Microbiol 87 (2021) e03109-20. https://doi.org/10.1128/AEM.03109-20.
[23] G. Ceriotti, A. Bosco-Santos, S.M. Borisov, J.S. Berg, Microbial iron reduction under oxic conditions: implications for subsurface biogeochemistry, (2024). https://doi.org/10.48550/arXiv.2404.07137.
[24] T. Shi, C. Peng, L. Lu, Z. Yang, Y. Wu, Z. Wang, A. Kappler, Response of Fe(III)-reducing kinetics, microbial community structure and Fe(III)-related functional genes to Fe(III)-organic matter complexes and ferrihydrite in lake sediment, Biogeochemistry 167 (2024) 1553–1565. https://doi.org/10.1007/s10533-024-01186-4.
[25] J.V. Boas, V.B. Oliveira, M. Simões, A.M.F.R. Pinto, Review on microbial fuel cells applications, developments and costs, Journal of Environmental Management 307 (2022) 114525. https://doi.org/10.1016/j.jenvman.2022.114525.
[26] J.M. Byrne, N. Klueglein, C. Pearce, K.M. Rosso, E. Appel, A. Kappler, Redox cycling of Fe(II) and Fe(III) in magnetite by Fe-metabolizing bacteria, Science 347 (2015) 1473–1476. https://doi.org/10.1126/science.aaa4834.
[27] C. Bryce, N. Blackwell, C. Schmidt, J. Otte, Y. Huang, S. Kleindienst, E. Tomaszewski, M. Schad, V. Warter, C. Peng, J.M. Byrne, A. Kappler, Microbial anaerobic Fe(II) oxidation –

Ecology, mechanisms and environmental implications, Environmental Microbiology 20 (2018) 3462–3483. https://doi.org/10.1111/1462-2920.14328.
[28] L. Liu, C. Zhu, M. Fan, C. Chen, Y. Huang, Q. Hao, J. Yang, H. Wang, D. Sun, Oxidation and degradation of graphitic materials by naphthalene-degrading bacteria, Nanoscale 7 (2015) 13619–13628. https://doi.org/10.1039/C5NR02502H.
[29] C. Zhu, L. Liu, M. Fan, L. Liu, B. Dai, J. Yang, D. Sun, Microbial oxidation of graphite by Acidithiobacillus ferrooxidans CFMI-1, RSC Adv. 4 (2014) 55044–55047. https://doi.org/10.1039/C4RA09827G.
[30] J. Wang, Q. Ma, Z. Zhang, S. Li, C.S. Diko, C. Dai, H. Zhang, Y. Qu, Bacteria mediated Fenton-like reaction drives the biotransformation of carbon nanomaterials, Science of The Total Environment 746 (2020) 141020. https://doi.org/10.1016/j.scitotenv.2020.141020.
[31] Y. Gu, M.J. Guberman-Pfeffer, V. Srikanth, C. Shen, F. Giska, K. Gupta, Y. Londer, F.A. Samatey, V.S. Batista, N.S. Malvankar, Structure of Geobacter cytochrome OmcZ identifies mechanism of nanowire assembly and conductivity, Nat Microbiol 8 (2023) 284–298. https://doi.org/10.1038/s41564-022-01315-5.
[32] F. Wang, C.H. Chan, V. Suciu, K. Mustafa, M. Ammend, D. Si, A.I. Hochbaum, E.H. Egelman, D.R. Bond, Structure of Geobacter OmcZ filaments suggests extracellular cytochrome polymers evolved independently multiple times, eLife 11 (2022) e81551. https://doi.org/10.7554/eLife.81551.
[33] E.C. Salas, Z. Sun, A. Lüttge, J.M. Tour, Reduction of Graphene Oxide via Bacterial Respiration, ACS Nano 4 (2010) 4852–4856. https://doi.org/10.1021/nn101081t.
[34] G. Wang, F. Qian, C.W. Saltikov, Y. Jiao, Y. Li, Microbial reduction of graphene oxide by Shewanella, Nano Res. 4 (2011) 563–570. https://doi.org/10.1007/s12274-011-0112-2.
[35] C.E.A. Engel, D. Vorländer, R. Biedendieck, R. Krull, K. Dohnt, Quantification of microaerobic growth of Geobacter sulfurreducens, PLOS ONE 15 (2020) e0215341. https://doi.org/10.1371/journal.pone.0215341.
[36] C. Sun, Y. Feng, Y. Li, C. Qin, Q. Zhang, W. Feng, Solvothermally exfoliated fluorographene for high-performance lithium primary batteries, Nanoscale 6 (2014) 2634–2641. https://doi.org/10.1039/C3NR04609E.
[37] M.C. Vu, N.A. Thi Thieu, J.-H. Lim, W.-K. Choi, J. Chan Won, Md.A. Islam, S.-R. Kim, Ultrathin thermally conductive yet electrically insulating exfoliated graphene fluoride film for high performance heat dissipation, Carbon 157 (2020) 741–749. https://doi.org/10.1016/j.carbon.2019.10.079.
[38] J.M. Byrne, H. Muhamadali, V.S. Coker, J. Cooper, J.R. Lloyd, Scale-up of the production of highly reactive biogenic magnetite nanoparticles using Geobacter sulfurreducens, Journal of The Royal Society Interface 12 (2015) 20150240. https://doi.org/10.1098/rsif.2015.0240.
[39] H. Koolivand, S. Mazinani, F. Sharif, Surface activity of N-graphene quantum dot in presence of CTAB surfactant, Surfaces and Interfaces 37 (2023) 102714. https://doi.org/10.1016/j.surfin.2023.102714.
[40] K. Inoue, X. Qian, L. Morgado, B.-C. Kim, T. Mester, M. Izallalen, C.A. Salgueiro, D.R. Lovley, Purification and Characterization of OmcZ, an Outer-Surface, Octaheme *c* -Type Cytochrome Essential for Optimal Current Production by *Geobacter sulfurreducens*, Appl Environ Microbiol 76 (2010) 3999–4007. https://doi.org/10.1128/AEM.00027-10.
[41] C. Zhu, S. Yang, G. Wang, R. Mo, P. He, J. Sun, Z. Di, Z. Kang, N. Yuan, J. Ding, G. Ding, X. Xie, A new mild, clean and highly efficient method for the preparation of graphene quantum dots without by-products, J. Mater. Chem. B 3 (2015) 6871–6876. https://doi.org/10.1039/C5TB01093D.
[42] Y. Li, Y. Hu, Y. Zhao, G. Shi, L. Deng, Y. Hou, L. Qu, An Electrochemical Avenue to Green-Luminescent Graphene Quantum Dots as Potential Electron-Acceptors for Photovoltaics, Advanced Materials 23 (2011) 776–780. https://doi.org/10.1002/adma.201003819.
[43] S. Lai, Y. Jin, L. Shi, R. Zhou, Y. Zhou, D. An, Mechanisms behind excitation- and concentration-dependent multicolor photoluminescence in graphene quantum dots, Nanoscale 12 (2020) 591–601. https://doi.org/10.1039/C9NR08461D.

[44] U. Rajeena, M. Akbar, P. Raveendran, R.M. Ramakrishnan, Fluorographite to hydroxy graphene to graphene: a simple wet chemical approach for good quality graphene, New J. Chem. 42 (2018) 9658–9665. https://doi.org/10.1039/C8NJ01392F.
[45] K.N. Kudin, B. Ozbas, H.C. Schniepp, R.K. Prud'homme, I.A. Aksay, R. Car, Raman Spectra of Graphite Oxide and Functionalized Graphene Sheets, Nano Lett. 8 (2008) 36–41. https://doi.org/10.1021/nl071822y.
[46] D. López-Díaz, M. López Holgado, J.L. García-Fierro, M.M. Velázquez, Evolution of the Raman Spectrum with the Chemical Composition of Graphene Oxide, J. Phys. Chem. C 121 (2017) 20489–20497. https://doi.org/10.1021/acs.jpcc.7b06236.
[47] K.K.H. De Silva, P. Viswanath, V.K. Rao, S. Suzuki, M. Yoshimura, New Insight into the Characterization of Graphene Oxide and Reduced Graphene Oxide Monolayer Flakes on Si-Based Substrates by Optical Microscopy and Raman Spectroscopy, J. Phys. Chem. C 125 (2021) 7791–7798. https://doi.org/10.1021/acs.jpcc.1c01152.
[48] E. Dervishi, Z. Ji, H. Htoon, M. Sykora, S.K. Doorn, Raman spectroscopy of bottom-up synthesized graphene quantum dots: size and structure dependence, Nanoscale 11 (2019) 16571–16581. https://doi.org/10.1039/C9NR05345J.
[49] L. Tang, R. Ji, X. Cao, J. Lin, H. Jiang, X. Li, K.S. Teng, C.M. Luk, S. Zeng, J. Hao, S.P. Lau, Deep ultraviolet photoluminescence of water-soluble self-passivated graphene quantum dots, ACS Nano 6 (2012) 5102–5110. https://doi.org/10.1021/nn300760g.
[50] H. Qin, T. Gong, Y. Jin, Y. Cho, C. Shin, C. Lee, T. Kim, Near-UV-emitting graphene quantum dots from graphene hydrogels, Carbon 94 (2015) 181–188. https://doi.org/10.1016/j.carbon.2015.06.033.
[51] V. Brusko, A. Khannanov, A. Rakhmatullin, A.M. Dimiev, Unraveling the infrared spectrum of graphene oxide, Carbon 229 (2024) 119507. https://doi.org/10.1016/j.carbon.2024.119507.
[52] A. Wang, S. Bok, C.J. Mathai, R. Thiruvengadathan, C.M. Darr, H. Chen, M.R. Zachariah, K. Gangopadhyay, J.A. McFarland, M.R. Maschmann, S. Gangopadhyay, Synthesis, characterization and nanoenergetic utilizations of fluorine, oxygen co-functionalized graphene by one-step XeF2 exposure, Combustion and Flame 215 (2020) 324–332. https://doi.org/10.1016/j.combustflame.2020.02.005.
[53] F. Zhou, Q. Dong, J.-T. Chen, B. Sengupta, J. Jiang, W.L. Xu, H. Li, S. Li, M. Yu, Printed graphene oxide-based membranes for gas separation and carbon capture, Chemical Engineering Journal 430 (2022) 132942. https://doi.org/10.1016/j.cej.2021.132942.
[54] D.S. Jensen, S.S. Kanyal, N. Madaan, M.A. Vail, A.E. Dadson, M.H. Engelhard, M.R. Linford, Silicon (100)/SiO2 by XPS, Surface Science Spectra 20 (2013) 36–42. https://doi.org/10.1116/11.20121101.
[55] R. Stine, W.-K. Lee, K.E. Whitener, J.T. Robinson, P.E. Sheehan, Chemical stability of graphene fluoride produced by exposure to XeF2, Nano Lett 13 (2013) 4311–4316. https://doi.org/10.1021/nl4021039.
[56] X. Chen, X. Wang, D. Fang, A review on C1s XPS-spectra for some kinds of carbon materials, Fullerenes, Nanotubes and Carbon Nanostructures 28 (2020) 1048–1058. https://doi.org/10.1080/1536383X.2020.1794851.
[57] A.P. Dementjev, A.V. Eletskii, K.I. Maslakov, E.G. Rakov, V.F. Sukhoverhov, A.V. Naumkin, Fluorination of Carbon Nanostructures and Their Comparative Investigation by XPS and XAES Spectroscopy, Fullerenes, Nanotubes and Carbon Nanostructures 14 (2006) 287–296. https://doi.org/10.1080/15363830600663990.
[58] H. Li, G. Hou, X. Yuan, Z. Liu, W. Luo, Y. Song, S. Bi, KOH modification of fluorinated graphite and its reaction mechanism, Front. Mater. 9 (2022). https://doi.org/10.3389/fmats.2022.999753.
[59] P. Gong, K. Hou, X. Ye, L. Ma, J. Wang, S. Yang, Synthesis of highly luminescent fluorinated graphene quantum dots with tunable fluorine coverage and size, Materials Letters 143 (2015) 112–115. https://doi.org/10.1016/j.matlet.2014.12.058.
[60] P. Gong, Z. Yang, W. Hong, Z. Wang, K. Hou, J. Wang, S. Yang, To lose is to gain: Effective synthesis of water-soluble graphene fluoroxide quantum dots by sacrificing certain fluorine atoms from exfoliated fluorinated graphene, Carbon 83 (2015) 152–161. https://doi.org/10.1016/j.carbon.2014.11.027.

[61] W. Lai, Y. Yuan, X. Wang, Y. Liu, Y. Li, X. Liu, Radical mechanism of a nucleophilic reaction depending on a two-dimensional structure, Phys. Chem. Chem. Phys. 20 (2017) 489–497. https://doi.org/10.1039/C7CP06708A.
[62] A. Sahu, J.R. Alston, C. Carlin, M. Craps, K. Davis, H.B. Harrison, T. Kongruengkit, A. Manikonda, S. Elmore, R. Rollins, B. Sadiku, S. Schmal, J. Shajahan, J.C. Poler, Fluorographite Nanoplatelets with Covalent Grafting of Anion-Exchange Resins for Water Purification, ACS Appl. Nano Mater. 5 (2022) 5709–5721. https://doi.org/10.1021/acsanm.2c00709.
[63] R. Yaokawa, K. Mukai, T. Nonaka, S. Kosaka, N. Ogihara, Redox Reaction Mechanism of Graphite Fluoride (CF)n in Fluoride-Ion Batteries, Chem. Mater. 35 (2023) 10584–10593. https://doi.org/10.1021/acs.chemmater.3c02217.
[64] C.I. Torres, R. Krajmalnik-Brown, P. Parameswaran, A.K. Marcus, G. Wanger, Y.A. Gorby, B.E. Rittmann, Selecting Anode-Respiring Bacteria Based on Anode Potential: Phylogenetic, Electrochemical, and Microscopic Characterization, Environ. Sci. Technol. 43 (2009) 9519–9524. https://doi.org/10.1021/es902165y.
[65] A.S. Commault, G. Lear, M.A. Packer, R.J. Weld, Influence of anode potentials on selection of Geobacter strains in microbial electrolysis cells, Bioresource Technology 139 (2013) 226–234. https://doi.org/10/f45c3k.